

1      **Detection of slow slip events using wavelet analysis of  
2      GNSS recordings**

3      **A. Ducellier<sup>1</sup>, K. C. Creager<sup>1</sup>, D. A. Schmidt<sup>1</sup>**

4      <sup>1</sup>University of Washington

5      **Key Points:**

- 6      • enter point 1 here  
7      • enter point 2 here  
8      • enter point 3 here

9      **Abstract**

10 Slow slip events were discovered in many subduction zones during the last two decades  
 11 thanks to recordings of the displacement of Earth's surface by dense Global Navigation  
 12 Satellite System (GNSS) networks. Slow slip can last from a few days to several years  
 13 and has a relatively short recurrence time (months to years), compared to the recurrence  
 14 time of regular earthquakes (up to several hundreds of years), allowing scientists to ob-  
 15 serve and study many complete event cycles. In many places, tectonic tremor is also ob-  
 16 served in relation to slow slip and can be used as a proxy to study slow slip events of mod-  
 17 erate magnitude where surface deformation is hidden in GNSS noise. However, in sub-  
 18 duction zones where no clear relationship between tremor and slow slip occurrence is ob-  
 19 served, these methods cannot be applied, and we need other methods to be able to bet-  
 20 ter detect and quantify slow slip. Wavelets methods such as the Discrete Wavelet Trans-  
 21 form (DWT) and the Maximal Overlap Discrete Wavelet Transform (MODWT) are math-  
 22 ematical tools for analyzing time series simultaneously in the time and the frequency do-  
 23 main by observing how weighted averages of a time series vary from one averaging pe-  
 24 riod to the next. In this paper, we use wavelet methods to analyze GNSS time series and  
 25 seismic recordings of slow slip events in Cascadia. We use detrended GNSS data, apply  
 26 the MODWT transform and stack the wavelet details over several nearby GNSS stations.  
 27 As an independent check on the timing of slow slip events, we also compute the cumu-  
 28 lative number of tremor in the vicinity of the GNSS stations, detrend this signal, and  
 29 apply the MODWT transform. In both time series, we can then see simultaneous wave-  
 30 forms whose timing corresponds to the timing of slow slip events. We assume that there  
 31 is a slow slip event whenever there is a peak in the wavelet signal. We verify that there  
 32 is a good correlation between slow slip events detected with only GNSS data, and slow  
 33 slip events detected with only seismic data. The wavelet-based detection method detects  
 34 all events of magnitude higher than 6 as determined by independent event catalogs (e.g.  
 35 (Michel, Gualandi, & Avouac, 2019)).

36      **1 Introduction**

37 Slow slip events are a new feature discovered in the last two decades in many sub-  
 38 duction zones thanks to recordings of the displacement of Earth's surface by dense Global  
 39 Navigation Satellite System (GNSS) networks. As with ordinary earthquakes, slow slip  
 40 events are caused by slip on a fault, such as the plate boundary between a tectonic plate  
 41 subducting under another tectonic plate. However, they take a much longer time (sev-  
 42 eral days to several years) to happen relative to ordinary earthquakes, and they have a  
 43 relatively short recurrence time (months to years), compared to the recurrence time of  
 44 regular earthquakes (up to several hundreds of years), allowing scientists to observe and  
 45 study many complete event cycles, which is typically not possible to explore with tra-  
 46 ditional earthquake catalogs (Beroza & Ide, 2011). A slow slip event on the plate bound-  
 47 ary is inferred to happen when there is a reversal of the direction of motion at GNSS sta-  
 48 tions, compared to the secular interseismic motion. Slow slip events have been observed  
 49 in many subduction zones, such as Cascadia, Nankai (southwest Japan), Alaska, Costa  
 50 Rica, Mexico, and New Zealand (Audet & Kim, 2016; Beroza & Ide, 2011).

51 In many places, tectonic tremor are also observed in relation to slow slip. Tremor  
 52 is a long (several seconds to many minutes), low amplitude seismic signal, with emer-  
 53 gent onsets, and an absence of clear impulsive phases. Tectonic tremor have been explained  
 54 as a swarm of small, low-frequency earthquakes (LFEs) (Shelly, Beroza, & Ide, 2007),  
 55 that is small magnitude earthquakes ( $M \sim 1$ ), for which frequency content (1-10 Hz) is  
 56 lower than for ordinary earthquakes (up to 20 Hz). In subduction zones such as Nankai  
 57 and Cascadia, tectonic tremor observations are spatially and temporally correlated with  
 58 slow slip observations (Obara, 2002; Rogers & Dragert, 2003). Due to this correlation,  
 59 these paired phenomena have been called Episodic Tremor and Slip (ETS). However, this  
 60 is not always the case. For instance, in northern New Zealand, tremor are more challeng-  
 61 ing to detect, and seem to be located downdip of the slow slip on the plate boundary.

In Cascadia and Guerrero, Mexico, tremor has been used as a proxy to observe slow slip events that are not directly detectable in the GNSS data. For instance, Aguiar, Melbourne, and Scrivner (2009) studied 23 ETS events in Cascadia with more than 50 hours of tectonic tremor. For all these events, they computed both the GPS-estimated moment release and the cumulative number of hours of tectonic tremor recorded. They observed a linear relationship between moment release and number of hours of tremor for ETS events of moment magnitude 6.3 to 6.8. They also observed many smaller bursts of tremor of duration 1 to 50 hours in between the big ETS events, without any detectable signal in the GPS data. However, based on the relationship between slow slip moment and number of hours of tremor for bigger events, it is possible to infer the existence of smaller slow slip events of magnitude 5-6 occurring simultaneously with the tremor bursts. This leads to a power-law relationship between seismic moment and number of events with a *b*-value close to one, similar to the distribution of normal earthquakes ([reference?](#)).

Frank (2016) divided GPS time series observations into two groups: the first group contains days when slow seismicity (tectonic tremor and LFEs) is detected, the second group contains days when the numbers of tremor or LFEs is lower than a threshold. He then stacked separately the two groups of observations and observed a cumulative displacement in the northern direction (for Guerrero) and the eastern direction (for Cascadia) corresponding to the loading period when few tremor or LFEs are observed and the surface deformation corresponds to the secular plate motion. He also observed a cumulative displacement in the southern direction (for Guerrero) and the western direction (for Cascadia) corresponding to the release period when tremor and LFEs are observed. He was thus able to observe a reverse displacement corresponding to smaller slow slip events not directly observable in the GPS data.

However, in other subduction zones such as New Zealand, there is no clear relationship between tremor and slow slip occurrence and these methods cannot be applied to detect smaller slow slip events that produce a GNSS signal with an amplitude too small compared to the noise. We thus need other methods to be able to better detect and quantify slow slip.

Wavelets methods such as the Discrete Wavelet Transform (DWT) are mathematical tools for analyzing time series simultaneously in the time and the frequency domain by observing how weighted averages of a time series vary from one averaging period to the next. Wavelet methods have been widely used for geophysical applications (Kumar & Foufoula-Georgiou, 1997). However, few studies have used wavelet methods to analyze recordings of slow slip, and their scope was limited to the detection of the bigger (magnitude 6-7) short-term (a few weeks) events (Alba, Weldon, Livelybrooks, & Schmidt, 2019; Ohtani, McGuire, & Segall, 2010; Szeliga, Melbourne, Santillan, & Miller, 2008; Wei, McGuire, & Richardson, 2012).

Szeliga et al. (2008) determined the timing and the amplitude of 34 slow slip events throughout the Cascadia subduction zone between 1997 and 2005. They modeled the GPS time series by the sum of a linear trend, annual and biannual sinusoids representing seasonal effects, Heaviside step functions corresponding to earthquakes and hardware upgrades, and a residual signal. They then applied a Gaussian wavelet transform to the residual time series to get the exact timing of the slow slip at each GPS station. The idea is that the wavelet transform allows us to analyze the signal both in the time and the frequency domains. A sharp change in the signal will be localized and seen at all levels of the wavelet decomposition, contrary to what happens with the periodic sinusoids of the Fourier transform.

Instead of using wavelets in the time domain, Ohtani et al. (2010) used 2D wavelet functions in the spatial domain to detect slow slip events. They designed the Network Stain Filter (NSF) to detect transient deformation signals from large-scale geodetic arrays. They modeled the position of the GPS station by the sum of the secular velocity, a spatially coherent field, site-specific noise, reference frame errors, and observation errors. The spatial displacement field is modeled by the sum of basis wavelets with time-varying weights. Their method has been successfully used to detect a transient event in

117 the Boso peninsula, Japan, and a slow slip event in the Alaska subduction zone (Wei  
 118 et al., 2012).

119 Finally, Alba et al. (2019) used hourly water level records from four tide gauges  
 120 in the Juan de Fuca Straight and the Puget Sound to determine vertical displacements,  
 121 uplift rates between ETS events, and net uplift rates between 1996 and 2011. Their main  
 122 idea is that the tidal level measured at a given gauge is the sum of a noise component  
 123 at multiple timescales (tides, ocean and atmospheric noise) and an uplift signal due to  
 124 the ETS events. The noise component is assumed to be coherent between all tidal gauges,  
 125 while the uplift signal is different provided that the gauges are far enough from each other.  
 126 By stacking the tidal records, the uplift signals cancel each other while the noise signal  
 127 is amplified. By stacking the details of the DWT decomposition, instead of stacking the  
 128 raw tidal record, each of the components of the noise at different time scales is retrieved  
 129 and can then be removed from the raw records to obtain the uplift signal. The authors  
 130 were then able to clearly see a difference in uplift between the two tidal gauges at Port  
 131 Angeles and Port Townsend.

132 In our study, we use a similar approach with a different reasoning. We only stack  
 133 signals at nearby GPS stations, assuming that the longitudinal displacement due to the  
 134 ETS events will then be the same at each of the GPS stations considered. We suppose  
 135 that some of the noise component is different at each GPS station and will be eliminated  
 136 by the stacking. Finally, we suppose that the noise and the longitudinal displacement  
 137 due to the ETS events and the secular plate motion have different time scales, so that  
 138 the wavelet decomposition will act as a bandpass filter to retrieve the displacement sig-  
 139 nal and highlight the ETS events. We use wavelet methods to analyze GPS and seismic  
 140 recordings of slow slip events in Cascadia. Our objective is to verify that there is a good  
 141 correlation between slow slip events detected with only GNSS data, and slow slip events  
 142 detected with only seismic data. We thus want to demonstrate that the wavelet-based  
 143 detection method can be applied to detect slow slip events that may be currently un-  
 144 detected with standard methods.

## 145 2 Data

146 We focused our study on northwest Washington State. For the GNSS data, we used  
 147 the GPS time series provided by the Pacific Northwest Geodetic Array, Central Wash-  
 148 ington University. These are network solutions in ITRF2008 with phase ambiguities re-  
 149 solved. Solutions are computed with JPL/NASA orbits and satellite clocks. North, East,  
 150 and Vertical directions are available. However, as the direction of the secular plate mo-  
 151 tion is close to the East direction, we only used the East direction of the GPS time se-  
 152 ries for the data analysis, as it has the best signal-to-noise ratio. The wavelet method  
 153 works best with data with zero mean, and no sharp discontinuities, so we use the cleaned  
 154 dataset, that is GPS times series with linear trends, steps due to earthquakes or hard-  
 155 ware upgrades, and annual and semi-annual sinusoids signals simultaneously estimated  
 156 and removed following Szeliga, Melbourne, Miller, and Santillan (2004). For the seis-  
 157 mic data, we used the tremor catalog from [reference for the catalog](#). The following is to  
 158 be modified. the Pacific Northwest Seismic Network (PNSN) (Wech, 2010). Tremor were  
 159 detected and located using waveform envelope correlation and clustering and a centroid  
 160 location is available for every given five-minute time window when tremor was detected.  
 161 As the catalog starts in August 2009, we only looked at GPS data recorded in 2009 or  
 162 later.

## 163 3 Method

### 164 3.1 The Maximal Overlap Discrete Wavelet Transform

165 The Discrete Wavelet Transform (DWT) is an orthonormal transform that trans-  
 166 forms a time series  $X_t$  ( $t = 0, \dots, N - 1$ ) into a vector of wavelet coefficients  $W_i$  ( $i = 0, \dots, N - 1$ ).

If we denote  $J$  the level of the wavelet decomposition, and we have  $N = n*2^J$ , where  $n$  is some integer higher or equal to 1, the vector of wavelet coefficients can be decomposed into  $J$  wavelet vectors  $W_j$  of lengths  $\frac{N}{2}, \frac{N}{4}, \dots, \frac{N}{2^J}$ , and one scaling vector  $V_J$  of length  $\frac{N}{2^J}$ . Each wavelet vector  $W_j$  is associated with changes on scale  $\tau_j = dt2^{j-1}$ , where  $dt$  is the time step of the time series, and corresponds to the filtering of the original time series with a filter with nominal frequency interval  $[\frac{1}{dt2^{j+1}}; \frac{1}{dt2^j}]$ . The scaling vector  $V_J$  is associated with averages in scale  $\lambda_J = dt2^J$ , and corresponds to the filtering of the original time series with a filter with nominal frequency interval  $[0; \frac{1}{dt2^{j+1}}]$ . We can also define for  $j = 1, \dots, J$  the  $j$ th wavelet detail  $D_j$ , which is a vector of length  $N$ , and is associated to scale  $\tau_j = dt2^{j-1}$ . Similarly, we can define for  $j = 1, \dots, J$  the  $j$ th wavelet smooth  $S_j$ , which is a vector of length  $N$ , and is associated to scales  $\tau_{j+1} = dt2^{j+1}$  and higher. Together, the details and the smooths define the multiresolution analysis (MRA) of  $X$ :

$$X = \sum_{j=1}^J D_j + S_J \quad (1)$$

The DWT present several disadvantages. First, the length of the time series must be a multiple of  $2^J$  where  $J$  is the level of the DWT decomposition. Second, the time step of the wavelet vector  $W_j$  is  $dt2^j$ , which may not correspond to the time when some interesting phenomenon is visible on the original time series. Third, when we circularly shift the time series, the corresponding wavelet coefficients, details and smooths are not a circularly shifted version of the wavelet coefficients, details and smooths of the original time series. Thus, the values of the wavelet coefficients, details and smooths are strongly dependent on the time when we start experimentally gathering the data. Finally, when we filter the time series to obtain the details and smooths, we introduce a phase shift, which makes difficult to line up meaningfully the features of the MRA with the original time series.

This is why we use instead the Maximal Overlap Discrete Wavelet Transform (MODWT). The MODWT transforms the time series  $X_t$  ( $t = 0, \dots, N - 1$ ) into  $J$  wavelet vectors  $\tilde{W}_j$  ( $j = 1, \dots, J$ ) of length  $N$  and a scaling vector  $\tilde{V}_J$  of length  $N$ . As is the case for the DWT, each wavelet vector  $\tilde{W}_j$  is associated with changes on scale  $\tau_j = dt2^{j-1}$ , and corresponds to the filtering of the original time series with a filter with nominal frequency interval  $[\frac{1}{dt2^{j+1}}; \frac{1}{dt2^j}]$ . The scaling vector  $\tilde{V}_J$  is associated with averages in scale  $\lambda_J = dt2^J$ , and corresponds to the filtering of the original time series with a filter with nominal frequency interval  $[0; \frac{1}{dt2^{j+1}}]$ . As is the case for the DWT, we can write the MRA:

$$X = \sum_{j=1}^J \tilde{D}_j + \tilde{S}_J \quad (2)$$

The MODWT of a time series can be defined for any length  $N$ . The time step of the wavelet vectors  $\tilde{W}_j$  and the scaling vector  $\tilde{V}_J$  is equal to the time step of the original time series. When we circularly shift the time series, the corresponding wavelet vectors, scaling vector, details and smooths are shifted by the same amount. The details and smooths are associated with a zero phase filter, making it easy to line up meaningfully the features of the MRA with the original time series. The wavelet methods for time series analysis are explained in a more detailed way in (Percival & Walden, 2000)).

### 3.2 Application to synthetic data

To illustrate the wavelet transform method, we first apply the MODWT to synthetics data. As slow slip events occur in Cascadia on a regular basis, every twelve to eighteen months, we create a synthetic signal of period  $T = 500$  days. To reproduce

the ground displacement observed on the longitudinal component of GPS stations in Cascadia, we divide each period into two parts: In the first part of duration  $T - N$ , the displacement is linearly increasing and corresponds to the secular plate motion in the eastern direction; in the second part of duration  $N$ , the displacement is linearly decreasing and corresponds to a slow slip event on a reverse fault at depth triggering a ground displacement in the western direction. To see the effect of the magnitude of the slow slip event, we use different values for  $N = 5, 10, 20, 40$  days. Figure 1 shows the synthetics, the details of the wavelet decomposition for levels 1 to 10, and the smooth for the four durations of a slow slip event.

The ramp-like signal is transformed through the wavelet filtering into a waveform with first a positive peak and then a negative peak. The shape of the waveform is the same for every level of the wavelet decomposition, but the width of the waveform increases with the scale level. For the 8th level of the wavelet decomposition, the width of the waveform is nearly as large as the time between two events. At larger scales, the waveforms start to merge two contiguous events together, and make the wavelet decomposition less interpretable. For an event of duration 5 days, the wavelet details at levels higher than 3 have a larger amplitude than the wavelet details at lower scales. For an event of duration 10 days, the wavelet details at levels higher than 4 have a larger amplitude than the wavelet details at lower scales. For an event of duration 20 days, the wavelet details at levels higher than 5 have a larger amplitude than the wavelet details at lower scales. For an event of duration 40 days, the wavelet details at levels higher than 6 have a larger amplitude than the wavelet details at lower scales. Thus, the scale levels at which an event is being seen in the wavelet details give us an indication about the duration (and the magnitude) of the slow slip event. We expect the big slow slip events of magnitude 6-7 that last several weeks to start being visible at the level 5 of the wavelet decomposition, but to not be noticeable at lower time scales.

### 3.3 MODWT of GPS and tremor data

The DWT and MODWT methods must be used on a continuous time series, without gaps in the recordings. To deal with the gaps in the GNSS recordings, we simply replace the missing values by the sum of a straight line and a Gaussian noise component with mean zero and standard deviation equal to the standard deviation of the whole time series. The straight line starts at the mean of the five days before the gap and ends at the mean of the five days after the gap. We verify how the wavelet details may be affected by looking at a GPS time series without missing values and comparing the wavelet details with and without removing some data points. Station PGC5 has recorded during 1390 days between 2009 and 2013, without any missing values. We first computed the wavelet details without missing values. Then, we removed ten neighboring missing values, replaced them by the sum of the straight line and the Gaussian noise component, and computed the wavelet details with the replaced values. Figure 2 shows a comparison of the two wavelet details for two different locations of the missing values. We can see that there are visible differences in the time series itself, and in the details at the smallest levels of the wavelet decomposition. However, the differences between the wavelet details with and without missing values get smaller and smaller with increasing levels the details, and are barely visible for the levels we are mostly interested in (levels 6 and above). We thus conclude that we can easily replace the missing values in the GNSS time series without introducing false detections of slow slip events.

We then applied the wavelet filtering to real GPS data. Figure 3 shows the longitudinal displacement for GPS station PGC5, located in southern Vancouver Island, the details of the wavelet decomposition for levels 1 to 8, and the smooth. In the data, we can see a sharp drop in displacement whenever there is a slow slip event. For levels 5 to 8, we can see in the details a positive peak followed by a negative peak whenever there is a drop in displacement in the data. We thus verify that the wavelet method can detect slow slip events.

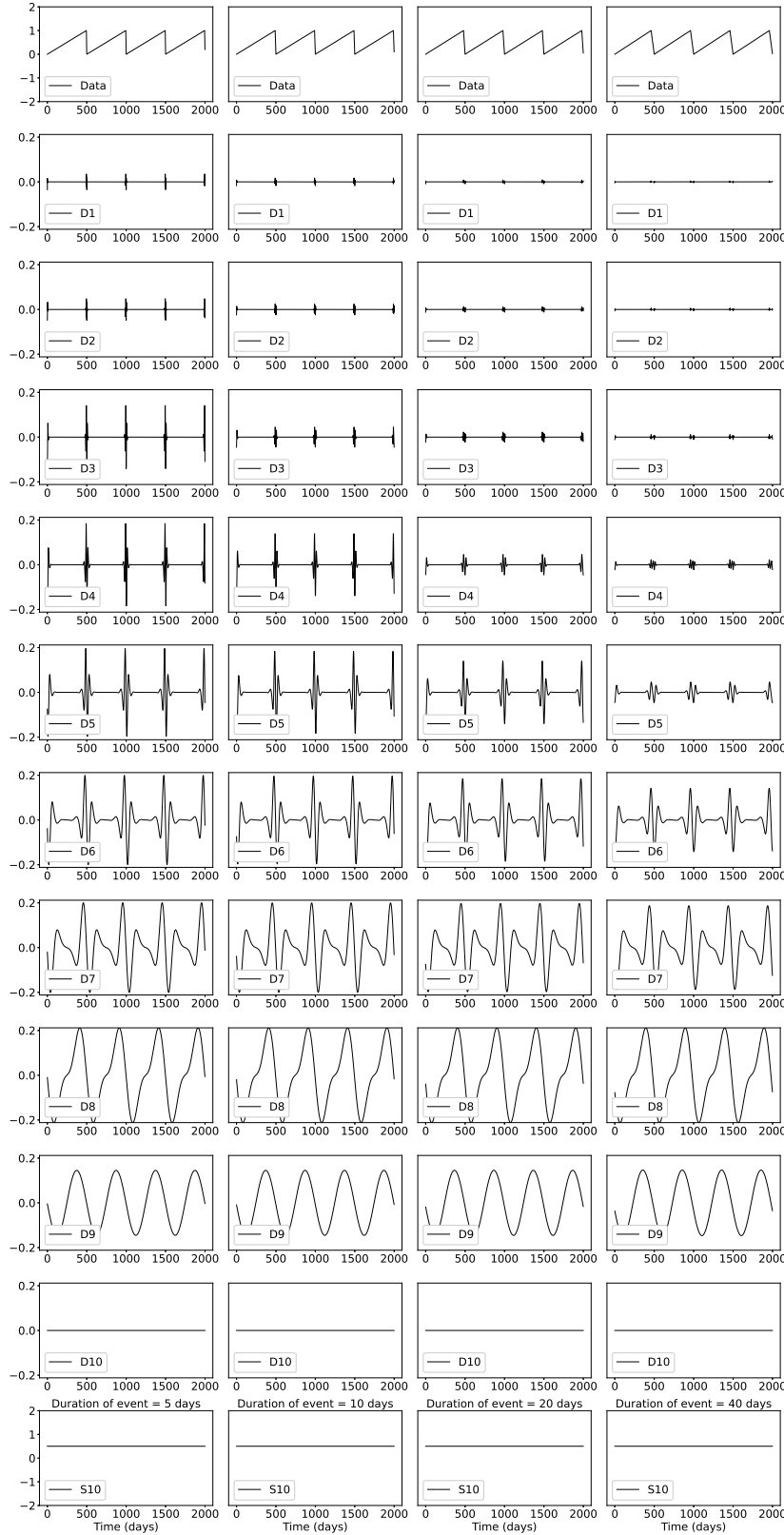


**Figure 1.** Details and smooth of the wavelet decomposition of a synthetics signal with period 500 days and duration of the slow slip event equal to 2 days (left), 5 days, 10 days, and 20 days (right).

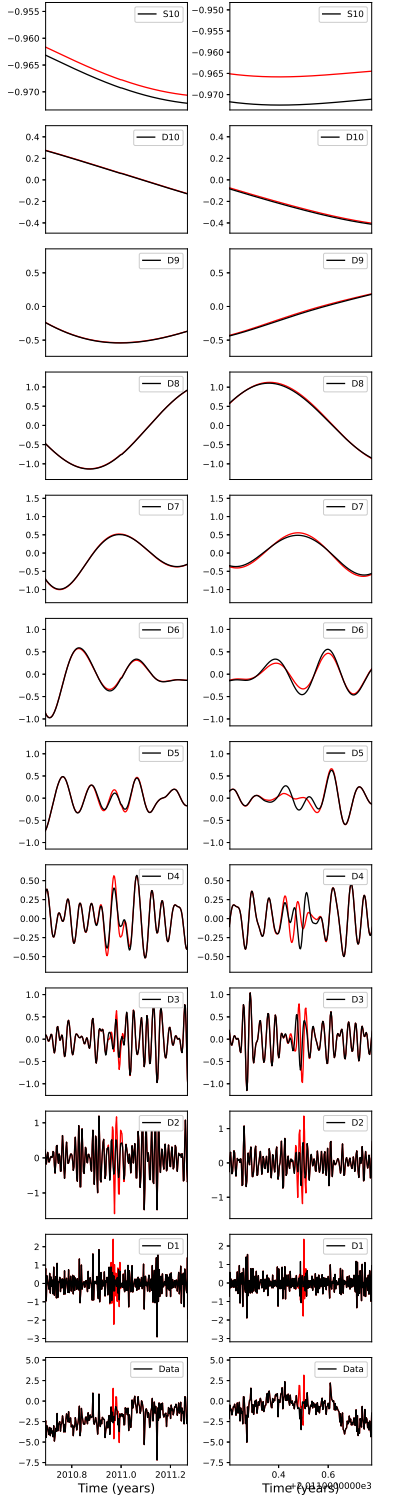


**Figure 2.** Bottom: Data from GPS station PGC5 without missing values (black) and with missing values replaced by the sum of a straight line and a Gaussian noise component (red) for two locations of the missing values (left and right). Bottom to top: Corresponding ten details and smooths of the wavelet composition for the original data (black) and for the missing values replaced by the sum of a straight line and a Gaussian noise component (red).

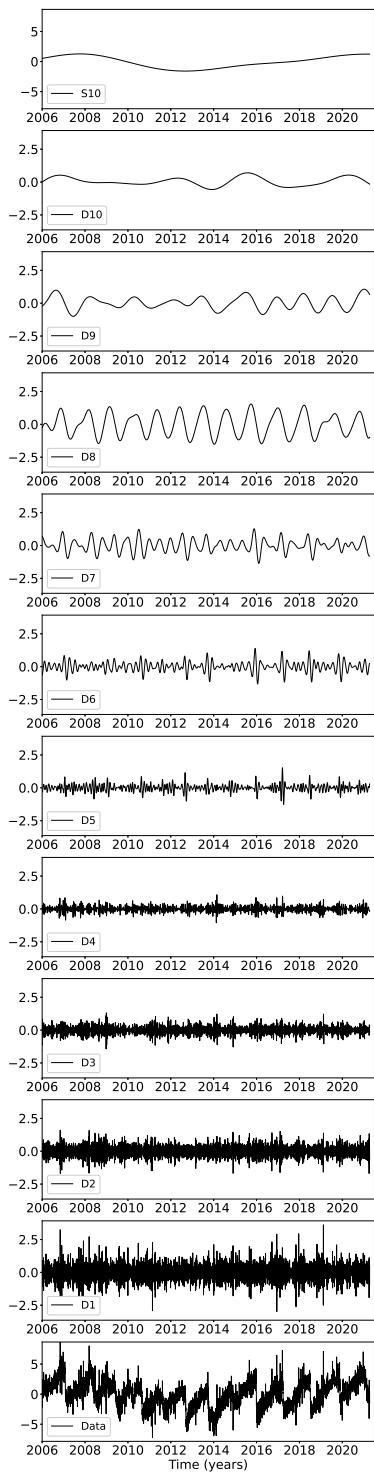


**Figure 3.** Details and smooth of the wavelet decomposition of the longitudinal displacement recorded at GPS station PGC5.

To increase the signal-to-noise ratio and be able to better detect slow slip events, we stack the signal over several GPS stations. We choose to focus on GPS stations located close enough to the tremor zone to get a sufficiently high amplitude of the slow slip signal. We choose 16 points located on the 40 km depth contour of the plate boundary (model from Preston, Creager, Crosson, Brocher, and Trehu (2003)) with spacing equal 0.1 degree in latitude (red triangles on Figure 4). Then we took all the GPS stations located in a 50 km radius for a given point, compute the wavelet details for the longitudinal displacement of each station, and stack each detail over the GPS stations. We thus have a stacked detail for each level 1 to 10 of the wavelet decomposition.

To compare slow slip events detected with GPS data and slow slip events detected with seismic data, we took all the tremor epicenters located within a 50 km radius centered on one of the 16 locations marked by red triangles on Figure 3. Then we computed the cumulative number of tremor within this circle. Finally, we removed a linear trend from the cumulative tremor count, and applied the wavelet transform. Figure 5 shows an example of the wavelet decomposition for the third northernmost location on Figure 4 (which is closest to GPS station PGC5). Contrary to what happens for the GPS data, we see a sharp increase in the data whenever there is a tremor episode, which translates into a negative peak followed by a positive peak in the wavelet details.

## 4 Results

We stacked the 8th level detail of the wavelet decomposition of the displacement over all the GPS stations located in a 50 km radius of a given point, for the 16 locations indicated in Figure 3. The result is shown in the top panel of Figure 6, where each line represents one of the locations. To better highlight the peaks in the wavelet details, we highlighted in red the time intervals where the amplitude of the stacked detail is higher than a threshold, and in blue the time intervals where the amplitude of the stacked detail is lower than minus the threshold. To compare the GPS signal with the tremor signal, we plotted the 8th level detail of the wavelet decomposition of the tremor count on the bottom panel of Figure 6. We used the opposite of the cumulative tremor count for the wavelet decomposition in order to be able to match positive peaks with positive peaks and negative peaks with negative peaks. In the tremor catalog from reference?, there are 17 tremor events with more than 150 hours of tremor recorded. The events are summarized in Table 1. The time of the event is the start date plus half the duration of the event. Although the latitudinal extension of the events is not always the same for the GPS data and for the tremor data, we identify the same 13 events in both 8th wavelet decompositions for the 8th level: January 2007, May 2008, May 2009, August 2010, August 2011, September 2012, September 2013, August-November 2014, January 2016, March 2017, June 2018, March-November 2019, and October 2020-January 2021. Although there are two events in the tremor catalog in August 2014 and November 2014, these two events are not distinguishable in the 8th level details and look more like a single event slowly propagating from South to North. The same phenomenon is observed in 2019 when two tremor events in March and November 2019 are merged into a single event propagating slowly from South to North. In 2020-2021, the wavelet decomposition of the tremor shows one event in the south in October-November 2020 and one event in the North in January 2021, but in the wavelet decomposition of the GPS data, these three events look like a single event propagating slowly from South to North.

Figures 7 and 8 show the same comparison between the wavelet decomposition of the GPS data and the wavelet decomposition of the tremor count data for the 7th level and the 6th level respectively. For the 7th level, we see the same events as for the 8th level, both for the GPS data and the tremor count data. The wavelet decomposition is more noisy for the GPS data between 2010 and 2012, but it does not seem that there are more slow slip events visible in the 7th level.

For the 6th level detail, we see an additional event in the South in Fall 2009 that is present both in the GPS and the tremor data. It may correspond to the northern ex-

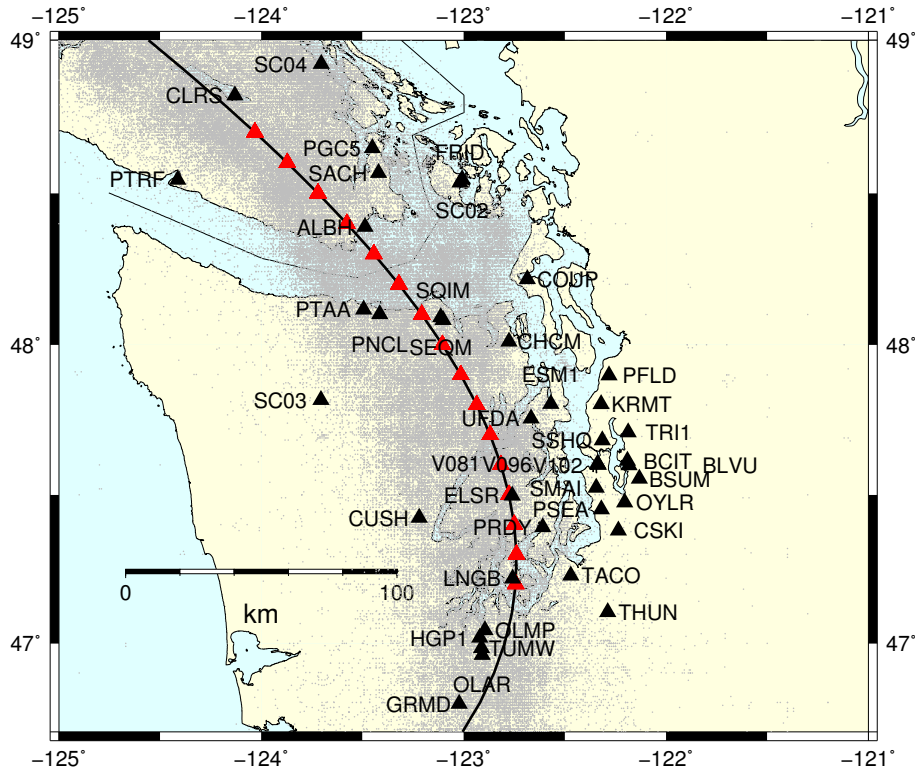


**Figure 4.** GPS stations used in this study (black triangles). The black line represents the 40 km depth contour of the plate boundary model by Preston et al. (2003). The red triangles are the locations where we stack the GPS data. The small grey dots are all the tremor locations from the PNSN catalog.

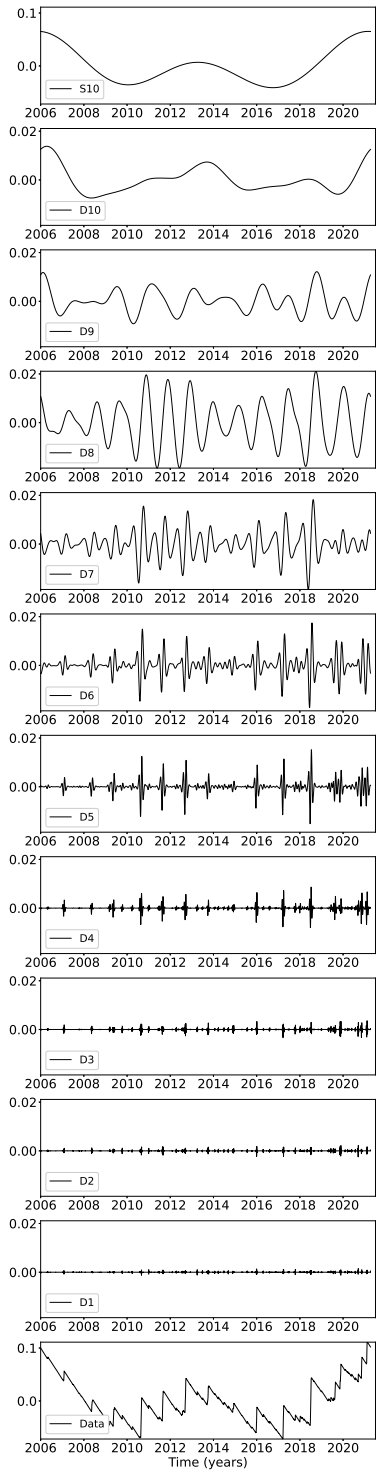


**Figure 5.** Details and smooth of the wavelet decomposition of the detrended cumulative tremor count around the third northernmost location on Figure 3.

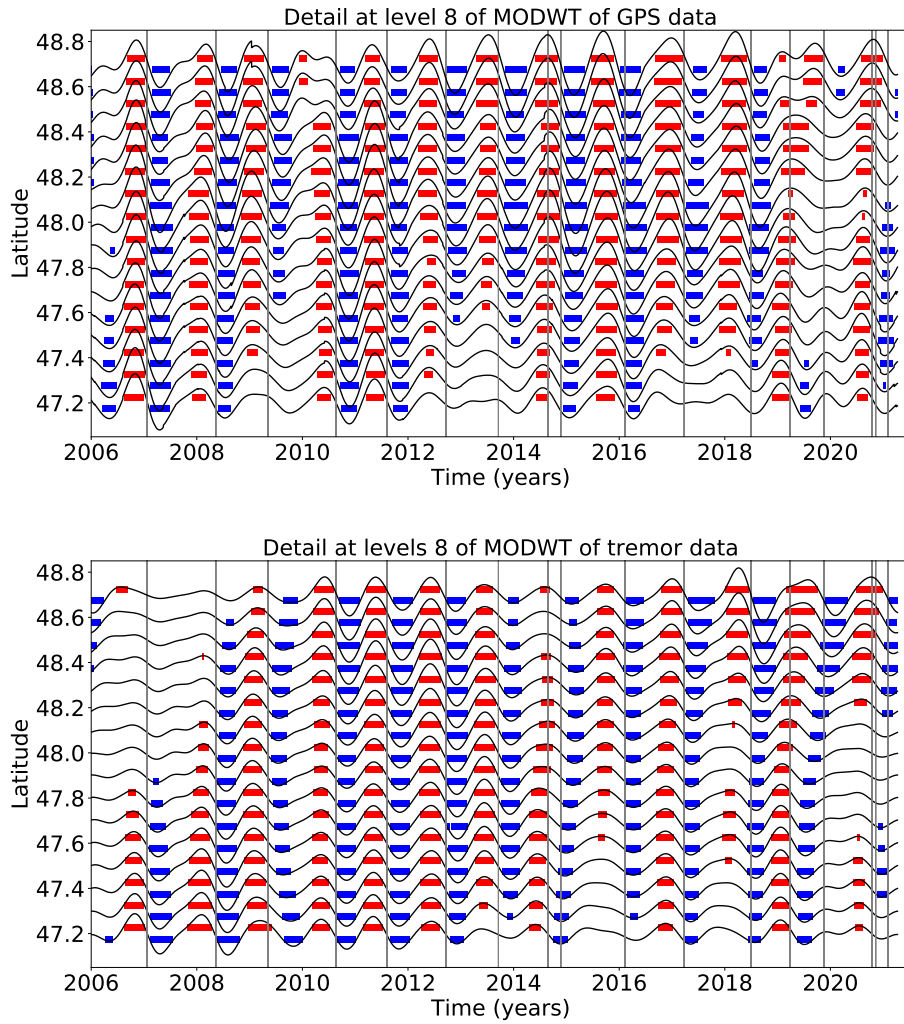


**Figure 6.** Top: Stacked 8th level details of the wavelet decomposition of the displacement over all the GPS stations located in a 50 km radius of a given point, for the 16 locations indicated in Figure 3. Bottom: Opposite of the 8th level detail of the cumulative tremor count in a 50 km radius of a given point for the same 16 locations.

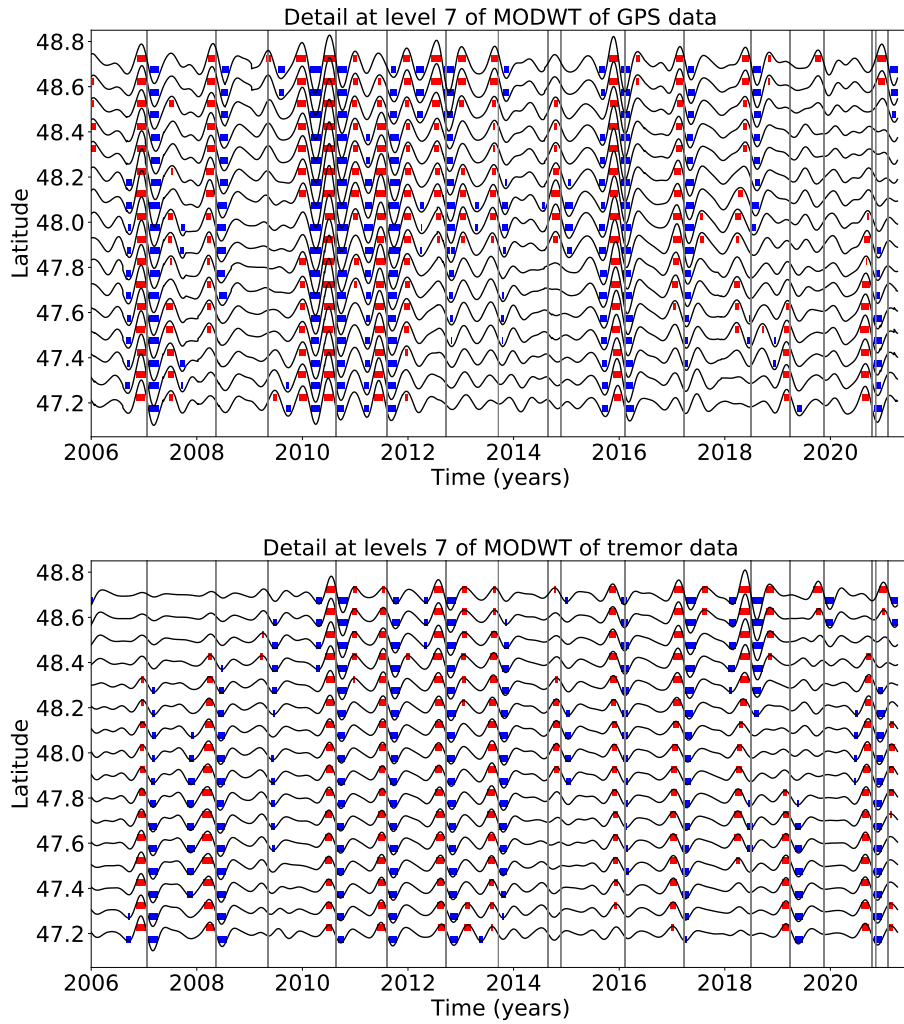


**Figure 7.** Top: Stacked 7th level details of the wavelet decomposition of the displacement over all the GPS stations located in a 50 km radius of a given point, for the 16 locations indicated in Figure 3. Bottom: Opposite of the 7th level detail of the cumulative tremor count in a 50 km radius of a given point for the same 16 locations.

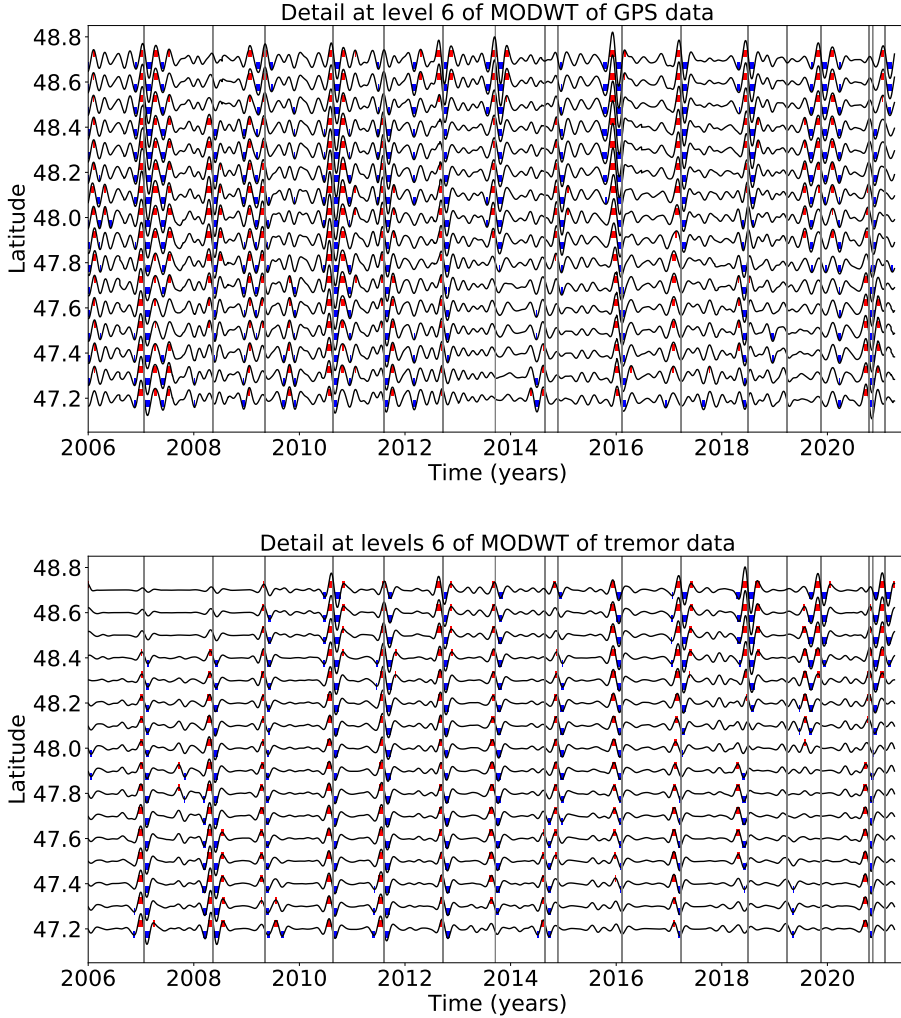


**Figure 8.** Top: Stacked 6th level details of the wavelet decomposition of the displacement over all the GPS stations located in a 50 km radius of a given point, for the 16 locations indicated in Figure 3. Bottom: Opposite of the 6th level detail of the cumulative tremor count in a 50 km radius of a given point for the same 16 locations.

tent of a big ETS event occurring in Fall 2009 south of the study area (event 19 in the Michel et al. (2019) catalog). There are three small signals in the GPS data in Spring 2012, Fall 2017, and Winter 2020 that are not present in the tremor data, and are probably false detections. To summarize, all the 13 events present on the 7th and 8th level details of the wavelet decomposition are true detections, 14 of the 17 events present on the 6th level detail of the wavelet decomposition are true detections.

## 5 Discussion

In addition to the magnitude 6 events discussed above, Michel et al. (2019) have also identified several magnitude 5 events using a variational Bayesian Independent Component Analysis (vbICA) decomposition of the signal. As we expect smaller magnitude events to be more visible at smaller time scales of the wavelet decomposition (level 5), we verify for all these events whether a signal can be seen at the same time as the time

**Table 1.** Big Episodic Tremor and Slip events. The duration and the number of tremor are from the tremor catalog of reference?. The event number and the magnitude are from the slow slip catalog of Michel et al. (2019).

Time	Duration (days)	Number of tremor (hours)	Event number	Magnitude
2007.06	28	398	3	6.68
2008.36	25	402	10	6.56
2009.35	24	248	16	6.49
2010.63	29	518	24	6.54
2011.60	37	479	30	6.47
2012.72	37	620	34	6.54
2013.71	27	423	41	6.58
2014.65	15	190	48	6.03
2014.89	38	385	51	6.40
2016.11	43	421	54	6.79
2017.23	19	279	59	6.61
2018.49	22	381		
2019.23	34	195		
2019.88	16	205		
2020.79	26	193		
2020.86	12	162		
2021.09	14	230		

given in their catalog. Most of these magnitude 5 events are also sub-events of bigger magnitude 6 events. Table 2 summarizes for each event its timing, its number and its magnitude as indicated in the catalog from Michel et al. (2019), and whether it is part of a bigger magnitude 6 event.

Figure 9 shows the 5th level detail wavelet decomposition of the GPS data. Red lines show the timing of the big ETS events from Table 1, and blue lines show the timing of the small slow slip events from Table 2.

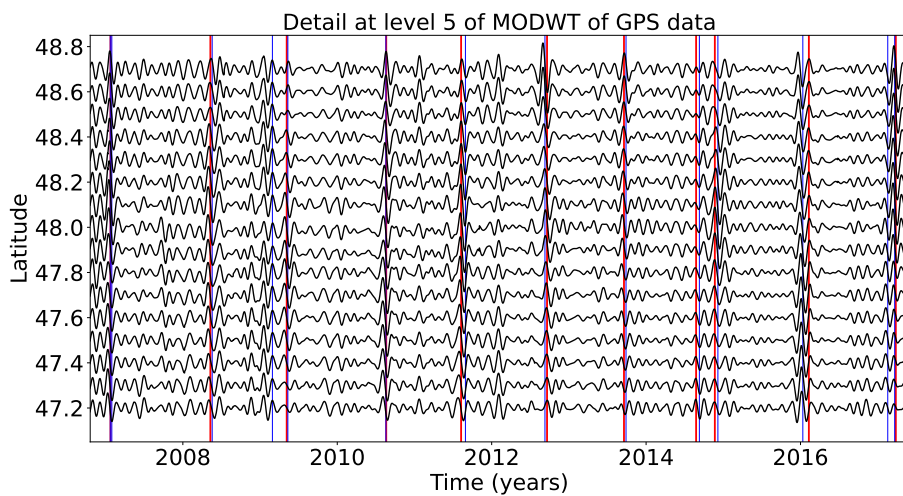
All 14 events that are sub-event of a bigger event are visible at level 5. However, this may be due because the bigger event are clearly seen at levels 6 to 8, and also at smaller time scales. The one small event that is not part of a bigger event (Winter 2009) is visible at level 5 of the wavelet decomposition. However, some other events that are not in Michel et al. (2019)'s catalog are also visible in late 2007, early 2010, early 2012, and late 2016. Therefore, it is difficult to make the difference between a true detection and a false detection, and to conclude whether the method can indeed detect events of magnitude 5.

## 6 Conclusion

In this paper, we have used wavelet methods to analyze GNSS time series and seismic recordings of slow slip events in Cascadia. We used detrended GNSS data, applied the MODWT transform and stack the wavelet details over several nearby GNSS stations. As an independent check on the timing of slow slip events, we also computed the cumulative number of tremor in the vicinity of the GNSS stations, detrended this signal, and applied the MODWT transform. In both time series, we could then see simultaneous waveforms whose timing corresponds to the timing of slow slip events. We assumed that there is a slow slip event whenever there is a peak in the wavelet signal. We verified that there is a good correlation between slow slip events detected with only GNSS data, and slow slip events detected with only seismic data. The wavelet-based detection method detects

**Table 2.** Magnitude 5 events from Michel et al. (2019).

Time	Event number	Magnitude	Sub-event of bigger event
2007.06	1	5.64	Yes
2007.08	2	5.91	Yes
2008.38	11	5.50	Yes
2009.16	14	5.50	No
2009.36	17	5.32	Yes
2010.63	25	5.76	Yes
2011.66	31	5.61	Yes
2011.66	32	5.32	Yes
2012.69	35	5.56	Yes
2013.74	42	5.71	Yes
2014.69	49	5.31	Yes
2014.93	52	5.39	Yes
2016.03	57	5.80	Yes
2017.13	60	5.43	Yes
2017.22	61	5.37	Yes

**Figure 9.** Top: Stacked 5th level details of the wavelet decomposition of the displacement over all the GPS stations located in a 50 km radius of a given point, for the 16 locations indicated in Figure 3.

356 all events of magnitude higher than 6 as determined by independent event catalogs (e.g.  
 357 (Michel et al., 2019)). We detected signals in the GPS data that could be magnitude 5  
 358 events, but it is not easy to make the difference between true detections and false de-  
 359 tections.

### 360 Acknowledgments

361 This work was funded by the grant from the National Science Foundation XXX. A.D.  
 362 would like to thank Pr Donald Percival for introducing her to wavelet methods during  
 363 his excellent class taught at University of Washington. The GPS recordings used for this  
 364 analysis can be downloaded from the PANGA website (GPS/GNSS Network and Geodesy  
 365 Laboratory: Central Washington University, other/seismic network, 1996). Figure 4 was  
 366 done using GMT (Wessel & Smith, 1991). The Python scripts used to analyze the data  
 367 and make the figures can be found on the first author's Github account.

### 368 References

- 369 Aguiar, A., Melbourne, T., & Scrivner, C. (2009). Moment release rate of Cascadia  
 tremor constrained by GPS. *Journal of Geophysical Research*, 114, B00A05.
- 370 Alba, S., Weldon, R. J., Livelybrooks, D., & Schmidt, D. A. (2019). Cascadia ETS  
 371 events seen in tidal records (1980–2011). *Bulletin of the Seismological Society  
 372 of America*.
- 373 Audet, P., & Kim, Y. (2016). Teleseismic constraints on the geological environ-  
 374 ment of deep episodic slow earthquakes in subduction zone forearcs: A review.  
 375 *Tectonophysics*, 670, 1-15.
- 376 Beroza, G., & Ide, S. (2011). Slow earthquakes and nonvolcanic tremor. *Annual Re-  
 377 view of Earth and Planetary Sciences*, 39, 271-296.
- 378 Frank, W. (2016). Slow slip hidden in the noise: The intermittence of tectonic re-  
 379 lease. *Geophysical Research Letters*, 43, 10125-10133.
- 380 GPS/GNSS Network and Geodesy Laboratory: Central Washington University,  
 381 other/seismic network. (1996). *Pacific Northwest Geodetic Array (PANGA)*.  
 382 International Federation of Digital Seismograph Networks. Retrieved from  
 383 <http://www.panga.cwu.edu/> doi: doi:10.7914/SN/PW
- 384 Kumar, P., & Foufoula-Georgiou, E. (1997). Wavelet analysis for geophysical appli-  
 385 cations. *Reviews of Geophysics*, 35(4), 385-412.
- 386 Michel, S., Gualandi, A., & Avouac, J.-P. (2019). Interseismic coupling and slow slip  
 387 events on the Cascadia megathrust. *Pure and Applied Geophysics*, 176, 3867-  
 388 3891.
- 389 Obara, K. (2002). Nonvolcanic deep tremor associated with subduction in southwest  
 390 Japan. *Science*, 296(5573), 1679-1681.
- 391 Ohtani, R., McGuire, J., & Segall, P. (2010). Network strain filter: A new tool for  
 392 monitoring and detecting transient deformation signals in GPS arrays. *Journal  
 393 of Geophysical Research*, 115, B12418.
- 394 Percival, D., & Walden, A. (2000). *Wavelet Methods for Time Series Analysis*. New  
 395 York, NY, USA: Cambridge University Press.
- 396 Preston, L., Creager, K., Crosson, R., Brocher, T., & Trehu, A. (2003). Intraslab  
 397 earthquakes: Dehydration of the Cascadia slab. *Science*, 302, 1197-1200.
- 398 Rogers, G., & Dragert, H. (2003). Tremor and slip on the Cascadia subduction zone:  
 399 The chatter of silent slip. *Science*, 300(5627), 1942-1943.
- 400 Shelly, D., Beroza, G., & Ide, S. (2007). Non-volcanic tremor and low-frequency  
 401 earthquake swarms. *Nature*, 446, 305-307.
- 402 Szeliga, W., Melbourne, T., Miller, M., & Santillan, V. (2004). Southern Cascadia  
 403 episodic slow earthquakes. *Geophysical Research Letters*, 31, L16602.
- 404 Szeliga, W., Melbourne, T., Santillan, M., & Miller, M. (2008). GPS constraints on  
 405 34 slow slip events within the Cascadia subduction zone, 1997-2005. *Journal of*

- 407           *Geophysical Research*, 113, B04404.  
408   Wech, A. (2010). Interactive tremor monitoring. *Seismological Research Letters*,  
409           81(4), 664-669.  
410   Wei, M., McGuire, J., & Richardson, E. (2012). A slow slip event in the south cen-  
411       tral Alaska Subduction Zone. *Geophysical Research Letters*, 39, L15309.  
412   Wessel, P., & Smith, W. H. F. (1991). Free software helps map and display data.  
413           *EOS Trans. AGU*, 72, 441.